Journal of Mechanical Science and Technology (KSME Int. J.), Vol. 19, No. 6, pp. 1347~1357, 2005 **1347**

Effects of Combustor-Level High Free-Stream Turbulence on Blade-Surface Heat/Mass Transfer in the Three-Dimensional Flow Region near the Endwall of a High-Turning Turbine Rotor Cascade

Sang Woo Lee*, Hyun Goo Kwon
School of Mechanical Engineering, Kumoh National Institute of Technology, Gumi, Gyongbook 730-701, Korea
Byung-Kyu Park
School of Mechanical and Aerospace Engineering, Seoul National University, Seoul 151-742, Korea

Effects of combustor-level high free-stream turbulence on the blade-surface heat/mass transfer have been investigated in the three-dimensional flow region near the endwall within a high-turning turbine rotor cascade passage. Free-stream turbulence intensity and integral length scale in the high turbulence case are 14.7 percents and 80 mm, respectively. The result shows that there is no considerable discrepancy in the blade heat/mass transfer near the endwall between the low and high turbulence cases. As departing from the endwall, however, the deviation between the two cases becomes larger, particularly in the region where flow separation and re-attachment occur. Under the high turbulence, flow disturbances such as boundary-layer separation and re-attachment seem to be suppressed, which makes the blade heat/mass transfer more uniform. Moreover, there are some evidences that endwall vortices tend to be weakened under the high turbulence.

Key Words : Gas Turbine, Turbin Rotor, Combustor-level Turbulence, Endwall Flow Region, Blade Surface Heat/Mass Transfer

Nomenclature

c : Chord length, Fig. 2
D : Diffusion coefficient of naphthalene in air
h_m : Local mass transfer coefficient
Nu : Nusselt number
Pr : Prandtl number, ν/α
Re : Inlet Reynolds number, $U_\infty c/\nu$
s : Span, Fig. 1
s_p, s_s : Curvilinear coordinates along the pressure and suction surfaces, Fig. 2
Sc : Schmidt number, ν/D
Sh : Sherwood number, $h_m c/D$
U_∞ : Inlet free-stream velocity
x_D, y_D, z_D : Coordinates at the inlet duct, Fig. 1
x, y, z : Cascade coordinates, Fig. 2

Greek Characters

α : Thermal diffusivity
ν : Kinematic viscosity

* Corresponding Author,
E-mail : swlee@kumoh.ac.kr
TEL : +82-54-467-4209; **FAX** : +82-54-467-4050
School of Mechanical Engineering, Kumoh National Institute of Technology, Gumi, Gyongbook 730-701, Korea. (Manuscript **Received** October 21, 2004; **Revised** May 4, 2005)

1. Introduction

For enhanced gas turbine performance, turbine durability problems due to hot gas temperature should be resolved. In general, a turbine blade usually suffers increased metal temperature and steeper temperature gradient. Contrary to two dimensionality of the mid-span flow, there exist very complicated three-dimensional vortex flows

near the endwall within a turbine blade passage. The endwall vortex flows tend to deliver more severe thermal loads to the blade surface. In order to design efficient cooling schemes for the entire turbine blade surface, a detailed description of the blade heat transfer coefficient near the endwall should be provided. The turbine blade is also exposed to very high inlet free-stream turbulence with a large length scale. Turbulence measurements taken at the exit of various gas turbine combustors have shown that the level can range between 8 and 40 percent (Koutmos and McGuirk, 1989; Goebel et al., 1993), which may have significant influences on the blade-surface thermal load.

Graziani et al.(1980) measured local Stanton numbers on an electrically-heated turbine endwall and blade surface for two different inlet boundary layers. They found that heat transfer is affected strongly by the passage vortex, and the inlet boundary-layer thickness on the endwall has a significant effect on the endwall and suction-surface heat transfer. Chen and Goldstein (1992) investigated turbulent transport on the suction surface of a turbine rotor blade at a low free-stream turbulence condition. They reported local heat/mass transfer data not only at the mid-span but also in the three-dimensional flow region near the endwall. Under low free-stream turbulence, Goldstein et al.(1995) measured detailed heat/mass transfer distributions in the three-dimensional flow region near the endwall of the pressure and suction surfaces of a turbine rotor blade.

Investigations on the blade heat transfer under high free-stream turbulence were conducted only at the mid-span. Bayley and Priddy (1981) investigated the effect of free-stream turbulence on the heat transfer in the two-dimensional flow region of a turbine rotor blade. They found that the laminar-turbulent transition on the surface significantly changes the heat transfer characteristics. Mehendale et al.(1994) reported free-stream turbulence effects on film effectiveness and heat transfer coefficient on a film-cooled turbine blade in the mid-span region. Wang et al.(1999) investigated effects of high free-stream turbulence on the heat/mass transfer at the mid-span of a turbine rotor cascade. Their results showed that the high free-stream turbulence and Reynolds number change the mid-span heat/mass transfer dramatically, and attention to turbulence length scale should be paid as well as turbulence intensity for better understanding.

In this study, the effects of combustor-level high free-stream turbulence on the entire blade-surface heat/mass transfer have been investigated for a high-turning turbine rotor blade, by using the naphthalene sublimation technique. This study is different from the previous ones, because the high turbulence effects are reported in the three-dimensional flow region near the endwall and the tested turbine blade has a higher turning angle.

2. Experiment

2.1 Cascade wind tunnel

As shown in Fig. 1, the cascade wind tunnel comprises an open-circuit type wind tunnel, a high turbulence generator, an inlet duct, a linear turbine cascade, and an exhaust section. The wind tunnel has a cross section of 0.6 m×0.4 m, and the inlet duct has a cross section of 0.42 m×0.32 m. The incoming flow is developing to a turbulent boundary-layer flow on the top and bottom walls of the inlet duct, after passing a trip wire of 1.8 mm and a sand paper. The linear turbine cascade has six large-scale turbine blades. They are fabricated based on the mid-span profile of a first-stage turbine rotor blade in an industrial gas turbine and are made of an engineering plastic

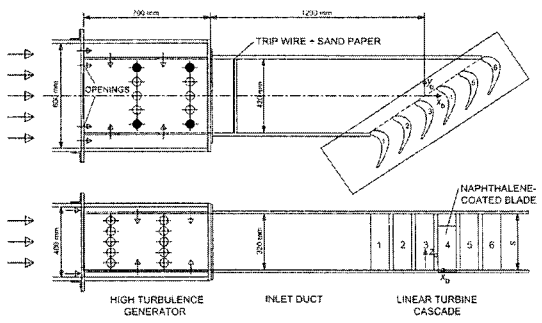

Fig. 1 Overall view of cascade wind tunnel

(Ivory MC Nylon). The blade profile is reported by Jun (2000).

The high turbulence generator is designed to simulate highly turbulent flow from a combustor. This has not only two side-plenums but also upper- and lower- plenums (Fig. 1). Two rows of five injection holes of 50 mm in diameter are drilled on the inside wall of each plenum. The main passage of the high turbulence generator is blocked partially at the inlet with an aluminum plate, so that the approaching flow can enter easily into the four plenums. Jets issuing into the main passage through the injection holes interact strongly with the main flows from the two front openings, and produce very high turbulence. The shaded holes in Fig. 1 indicate those blocked with tape for the most uniform distribution with a relatively high turbulence level at the exit (Lee et al., 2004).

As listed in Fig. 2, the chord length, c, axial chord, b, pitch, p, and span, s, are 217.8 mm, 196.0 mm, 151.6 mm, and 320.0 mm, respectively. The span is determined based on the span-to-chord ratio of the original rotor blade. The turning angle is given as 119 degrees, which is higher than those in the previous studies (Mehendale et al., 1994; Goldstein et al.,1995; Wang et al., 1999) by about 12 degrees. As shown in Fig. 2, x, y, and z are in the axial, pitch-wise and span-wise directions of the cascade, respectively. Two curvilinear coordinates, s_p and s_s, are defined along the blade surface as in Fig. 2. They start at an intersection of the blade profile with a line drawn upstream from the center of the leading-edge circle at the blade inlet angle.

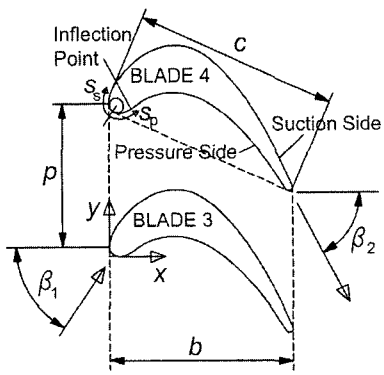

Number of blades	6
Chord length (c)	217.8 mm
Axial chord (b)	196.0 mm
Pitch (p)	151.6 mm
Span (s)	320.0 mm
Blade inlet angle (β_1)	56.4 deg
Blade outlet angle (β_2)	-62.6 deg

Fig. 2 Arrangement of turbine blade cascade

2.2 Naphthalene sublimation technique

In this technique, local mass transfer coefficient, h_m, is evaluated from the corresponding sublimation depth of cast naphthalene. The local Sherwood number is commonly used as a dimensionless mass transfer coefficient in the following way.

$$\mathrm{Sh}=\frac{h_m c}{D} \tag{1}$$

where D is the diffusion coefficient of naphthalene in air. According to the analogy between heat and mass transfer (Goldstein and Cho, 1995), the Nusselt number can be obtained as follows.

$$\frac{\mathrm{Nu}}{\mathrm{Sh}}=\left(\frac{\mathrm{Pr}}{\mathrm{Sc}}\right)^n \tag{2}$$

where n is usually taken to be 1/3 for a laminar boundary-layer flow and 0.4 for a turbulent one. The boundary condition in the mass transfer system is equivalent to the constant surface temperature condition in the heat transfer system.

A linear turbine blade coated with naphthalene and two molds are shown in Fig. 3. All of them

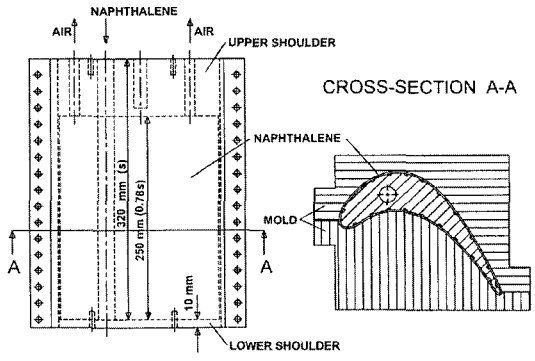

Fig. 3 Casting mold for naphthalene coated blade

are made of aluminum. Each mold has a well-polished inner surface, and they are bolted together when casting. The cast blade has upper and lower metal shoulders of which widths are 70 and 10 mm, respectively. A thin naphthalene layer of 2 mm in thickness is cast on the grooved recess of the cast blade between the two shoulders. The total length of the cast blade is 10 mm longer than the span. As in Fig. 1, the lower metal shoulder is inserted into an indentation machined on the bottom endwall of the cascade, so that the lower end of the naphthalene layer is flush mounted on the endwall surface. A T-type thermocouple is embedded in the cast naphthalene to obtain the naphthalene surface temperature during the sublimation experiment.

2.3 Four-axis profile measuring system

In order to measure sublimation depth on a turbine blade which has a varying local curvature around its surface, a depth gauge should be oriented normal to the surface. Thus, the present profile measuring system has not only a three-dimensional traversing mechanism for depth-gauge movement but also a blade rotator installed on a robust frame structure, as shown in Fig. 4. The rotating shaft is designed so as to prevent unnecessary shaft vibration during the rotation, and is driven by an AC servo motor (Oriental Motor, KXSM240HG1-BL) coupled with a harmonic reduction gear (Oriental Motor, UHG50-2C). This system prevents a backlash error and delivers an angle resolution of 0.0072 degrees. A hole drilled at the center of gravity of the cast blade is fitted to the upper portion of the shaft.

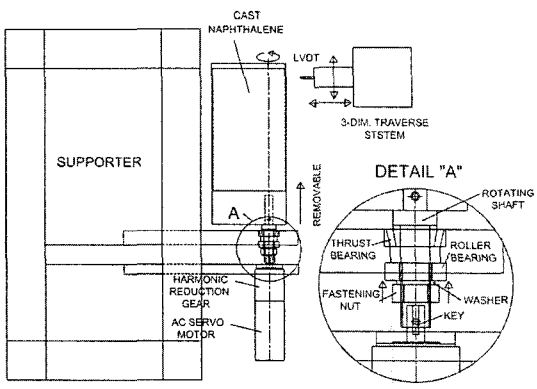

Fig. 4 Schematic diagram of four-axis profile measuring system

2.4 Data reduction system

Measurements of pressure, turbulence, temperature and naphthalene sublimation depth are controlled by a personal computer (IBM, Pentium) equipped with plug-in boards such as a Multi-Function DI/O Board (NI, AT-MIO-16D-H-9) and a GPIB adapter (NI, AT-GPIB). Temperatures of the free-stream and cast naphthalene are measured with T-type thermocouples connected to a digital voltmeter (Keithley, Model 2001TSCAN), which is controlled by the computer through the GPIB. The thermocouples are calibrated with a constant-temperature bath (Fisher Scientific, 9010) and a standard thermometer. Temperature measurements are based on the STP 470A (1974) published by ASTM. A LVDT (linear variable differential transformer) depth gauge (Sensortec, 060-3590-02) is used to measure local sublimation depth. Its full scale and resolution are ± 1.0 mm and 1.0 μm, respectively. In actual exposure experiments, average sublimation depth is maintained approximately at 0.1 mm, and maximum sublimation depth is less than about 0.3 mm. Sublimed depth is measured at 62 points around the blade and at 16 points in the span-wise or z-direction. The measurement locations are populated densely near the endwall as well as on the leading- and trailing-edges. During the scanning of the whole measurement locations, three sequential procedures of a precise rotation of the cast blade, which is followed by three-dimensional adjustment of the depth gauge, and then scans of it in the span-wise direction are repeated.

When a smooth solid surface of naphthalene is obtained, the test blade is mounted on the rotating shaft and is fixed with a bolt. Then, the first scanning of the naphthalene surface is conducted with the calibrated depth gauge, before exposure to the air flow. The readings of local elevation are recorded in the computer through the 12-bit A-D converter. Then, the cast blade is positioned in the cascade as in Fig. 1. After it is exposed

to the air flow for about 90 minutes, it is brought back to the profile measuring system, and is scanned again. The difference between the before-and-after readings at each location still includes free-convection loss during the setup time of the cast blade as well as during the depth measurements. This extra sublimation depth is typically about 7.3 percents of the average sublimation depth. The net sublimation depth is finally obtained after a proper correction.

2.5 Operating conditions and uncertainties

The inlet flow conditions in this study are summarized in Table 1. The free-stream velocity in the inlet duct is maintained at 15 m/s and the inlet Reynolds number based on the free-stream velocity and the chord length, Re, is 2.09×10^5. At $x_D/c=-1.5$, free-stream turbulence intensity is 0.3% in the low turbulence case, and free-stream turbulence intensity and integral length scale are 14.7% and 80 mm respectively in the high turbulence case. The boundary-layer thickness (δ_{99}), displacement thickness (δ_2), and momentum thickness (δ^*) at $x_D/c=-0.23$ are listed in Table 1. The momentum thickness in the high turbulence case is thinner than a half of that in the low turbulence case. We do not attempt to make the momentum thicknesses the same in the two cases, because thinning of an inlet boundary layer is one of the major effects of high inlet turbulence. During the sublimation experiments, the naphthalene surface temperature is monitored, and its variation is kept within 0.2℃. The uncertainty interval of the Sherwood number with 95 percent confidence based on Abernethy et al. (1985) is estimated to be ±7.0 percents.

Table 1 Operating conditions

	Free-Stream ($x_D/c=-1.5$)		Endwall Boundary Layer ($x_D/c=-0.23$)	
Low Turbulence Case	Re	2.09×10^5	δ_{99}	49.9 mm
	Tu	0.3%	δ_2	5.89 mm
	L	–	δ^*	4.59 mm
High Turbulence Case	Re	2.09×10^5	δ_{99}	26.8 mm
	Tu	14.7%	δ_2	2.26 mm
	L	80 mm	δ^*	1.89 mm

3. Results and Discussion

3.1 Local Sherwood number at the mid-span

Local Sherwood number distributions at the mid-span are presented in Fig. 5 in the low and high turbulence cases. For comparison with the previous result by Goldstein et al.(1995), the Sherwood number is expressed in the form of $Sh/Re^{0.5}$

The profile of $Sh/Re^{0.5}$ in the present low turbulence case shows various basic transport phenomena along the blade surface at the mid-span. $Sh/Re^{0.5}$ has a highest value at $s_p/c=0.0$. On the pressure surface, it sharply decreases and shows a local minimum at about $s_p/c=0.1$ due to a boundary-layer separation near the inflection point (Fig. 2). Then, it rapidly increases to reach a local maximum near $s_p/c=0.23$, which suggests flow re-attaching. After $s_p/c=0.23$, $Sh/Re^{0.5}$ decreases gradually as a result of subsequent boundary-layer development. It is known that the boundary layer on the pressure surface remains laminar even after the re-attachment (Goldstein et al., 1995). Then, $Sh/Re^{0.5}$ has another local minimum and local maximum resulted from a trailing-edge flow separation and a vortex shedding in turn. On the suction side, $Sh/Re^{0.5}$ near the leading edge also decreases sharply, and finally $Sh/Re^{0.5}$ has a local minimum of about 0.1 at $s_s/c=0.7$, which is the lowest value all over the pressure and suction sides. This trend is mainly attributed to a strong boundary-layer separation over the suction surface. Downstream of this minimum location, $Sh/Re^{0.5}$ turns to in-

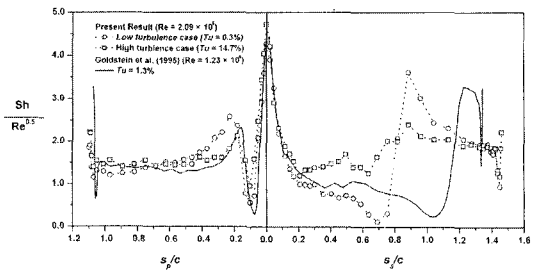

Fig. 5 Chord-wise distributions of $Sh/Re^{0.5}$ at mid-span

crease dramatically and reaches the value of 3.6. This steep increment is resulted from a strong re-attaching process after the separation, and is also due partly to a laminar-to-turbulent boundary-layer transition. Downstream of this peak, $Sh/Re^{0.5}$ tends to decrease again, but still has a higher value than that on pressure-side after $s_p/c=0.23$. Even just before the trailing-edge separation, $Sh/Re^{0.5}$ on the suction surface is 35 percent higher than that on the pressure surface. This fact means that there is a turbulent boundary layer on the suction surface after the peak at $s_s/c=0.9$. As found on the pressure side, there is a sharp decrease and a rapid recovery of $Sh/Re^{0.5}$ on the trailing edge.

The solid line found in Fig. 5 represents the mid-span results at $Tu=1.3$ percents by Goldstein et al.(1995). In general, the present result in the low turbulence case is very similar to theirs on the leading edge and over the pressure side. There is a good agreement in the highest values of $Sh/Re^{0.5}$ between two leading-edge peaks only within about 3 percents. In this study, $Sh/Re^{0.5}$ has its highest value at s_p/c or $s_s/c=0.0$. On the other hand, their highest value is found at $s_s/c=0.02$. This is resulted from the different origins of curvilinear coordinates. Their origin is positioned at a true stagnation point, but the present one is located at a geometric stagnation point as shown in Fig. 2. In general, the true stagnation point is situated slightly away from the geometrical one toward the pressure side (Lee et al., 2004). Over the suction surface, discrepancies become noticeable as moving downstream. Judging from the two low turbulence results, it is understood that their boundary-layer separation and subsequent re-attachment/transition are retarded significantly, compared with the present ones. The present turbine blade has a higher turning angle than theirs by about 12 degrees. Earlier separation in this study is due mainly to its high-turning blade profile. After the early re-attachment/transition, the present turbulent boundary layer has a chance to grow, meanwhile theirs immediately suffers a trailing-edge flow separation.

Mid-span $Sh/Re^{0.5}$ in the high turbulence case in Fig. 5 is compared with that in the present low turbulence case. Overall comparisons show that the difference between the two cases is most noticeable on the suction surface. Moreover, the high turbulence makes local mass transfer more uniform on both the pressure and suction surfaces, particularly in the regions where flow separation and re-attachment occur. Under the high free-stream turbulence, $Sh/Re^{0.5}$ at the stagnation point on the leading edge increases by about 8.4 percents, but $Sh/Re^{0.5}$ on the leading edge has nearly the same trend in both the low and high turbulence cases. On the pressure surface, the local minimum and subsequent maximum values near the inflection point under the high turbulence are higher and lower than the corresponding ones in the low turbulence case, respectively. In general, high turbulence with a large length scale provides an intense lateral mixing and a thinning effect on the boundary layer. As a result, flow disturbances such as flow separation and re-attachment are stabilized. This is why local variation is reduced near the inflection point. In the other regions on the pressure surface, however, the high turbulence has no considerable effects on $Sh/Re^{0.5}$. Therefore, it is inferred that the pressure-side boundary layer remains laminar even under the high turbulence. On the suction surface, the results in the low and high turbulence cases start to be deviated from each other at about $s_s/c=0.2$ and have nearly the same value again at about $s_s/c=1.2$. The noticeable decrease and following rapid increase in $Sh/Re^{0.5}$ after $s_s/c=0.2$ in the low turbulence case cannot be found in the high turbulence case. Instead, $Sh/Re^{0.5}$ in the high turbulence case has a much higher value near the separation point but has a much lower value around the re-attachment point, so that the distribution of Sh becomes more uniform under the high turbulence. This is because under the high turbulence, there seems to be no distinct boundary-layer separation and subsequent re-attachment process but seems to be a gradual transition from a laminar boundary layer to a turbulent one. After $s_s/c=1.2$, there is no big difference in $Sh/Re^{0.5}$ between the low and high turbulence cases, which shows that there are only

turbulent boundary layers in both the cases.

3.2 Local Sherwood number in the three-dimensional flow region

Contours of Sh on the pressure surface in the low and high turbulence cases are shown in Fig. 6. In the low turbulence case (Fig. 6(a)), Sh near the stagnation point has a steep gradient with higher values and its contours are in the form of a vertical straight line along the leading edge. In the range between $s_p/c=0.07$ and 0.13, Sh suffers a sudden decrease to a value lower than 400 due to the inflection-point flow separation. After this, Sh increases up to about 1200 as a result of flow re-attaching. Then, it decreases mildly until the trailing edge is reached, and finally a higher mass-transfer area is found on the trailing edge. These trends are not true for the mass transfer near the endwall. Along the endwall corner, contours of Sh are deviated from the vertical straight line even on the leading edge and become horizontal in the downstream region. This is resulted from the existence of secondary flows such as a pressure-side leading-edge horseshoe vortex, a pressure-side leading-edge corner vortex, and a pressure-side corner vortex along the downstream corner (Wang et al., 1997). The influence of these endwall vortices on the local mass transfer reaches the location of $z/s=0.1$.

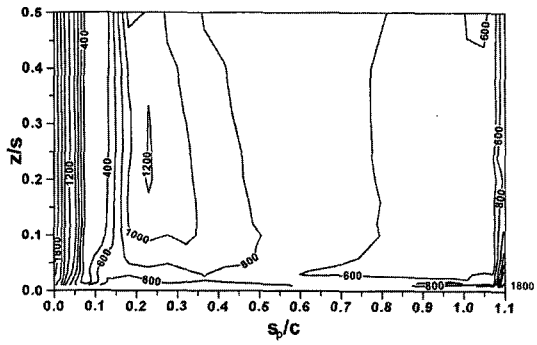

(a) Low turbulence case

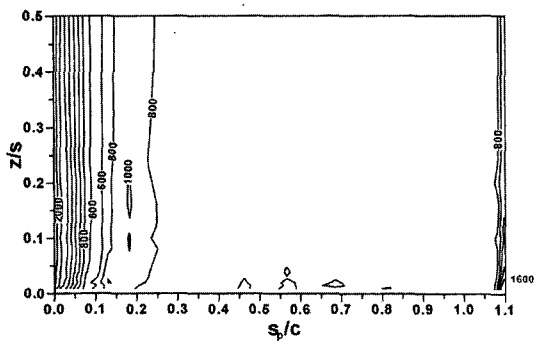

(b) High turbulence case

Fig. 6 Contours of Sh on the pressure surface

Contours of Sh on the pressure surface in the high turbulence case are presented in Fig. 6(b). In general, the high turbulence provides more uniform distribution of Sh even near the endwall, in comparison with the low turbulence case. This fact implies that the high turbulence tends to weaken the vortices near the endwall and to suppress the flow separation and subsequent re-attachment. The contours in the high turbulence case are so straight and vertical that mass transfer rate becomes nearly one-dimensional in the s_p-direction, regardless of z/s. In Fig. 6(b), contours are populated densely only in the leading- and trailing-edge regions. In the range of $0.25<s_p<1.05$, however, the high turbulence makes mass transfer remarkably uniform even near the endwall corner. This uniformity would be attributed to the lateral vigorous turbulent mixing. Close examinations of Fig. 6(a) and (b) reveals that there exist a considerable mass transfer and a steep gradient of Sh near the endwall corner at $s_p/c=1.1$. This high mass transfer is resulted from the strong interaction between the pressure-side corner vortex and vortex shedding. The peak value of Sh at this corner is nearly the same as that at the stagnation point in the low turbulence case. Under the high turbulence, however, the highest value of Sh is found at the leading-edge stagnation point as can be seen in Fig. 6(b).

Contours of Sh on the suction surface in the low turbulence case are presented in Fig. 7(a). Due to the strong boundary-layer separation and its re-attachment near the mid-chord as discussed in Fig. 5, Sh decreases consistently and then increases sharply at about $s_s/c=0.75$. After a local peak value at the re-attachment point, Sh decreases again. These phenomena are confined only to the mid-span area between $z/s=0.3$ and 0.5. Near the endwall on the suction side, there

is another high mass-transfer region. Curve A, which is drawn along a ridge of local mass transfer adjacent to the endwall, is considered as a trajectory of the suction-side corner vortex. The peak value of Sh near the endwall is situated on Curve A and is about 2200 which is highest all over the pressure and suction surfaces (Fig. 6(a) and Fig. 7(a)). Curve B is a locus along a valley of mass transfer. It is known that the secondary flow induced by the passage vortex departs from the suction surface along Curve B. Curve C connects the local maximum values outside of the passage vortex region and is an evidence of a new vortex. Wang et al.(1997) also found this trace and named a "wall vortex". It is clearly observed from Fig. 7(a) that a trace with steep gradient of Sh is in the form of an alphabet "D" over the entire suction surface.

Contours of Sh on the suction surface in the high turbulence case are provided in Fig. 7(b). The overall local mass-transfer distribution under the high turbulence shows the same trend as that in Fig. 7(a) in the near-endwall area as well as in the leading- and trailing-edge regions. However, the steep-gradient trace in the form of an alphabet "D" in Fig. 7(a) is hardly found in the high turbulence case, although a contour of Sh=800 in Fig. 7(b) is still observed in the same form. This implies that the strong flow separation and subsequent re-attachment in the low turbulence case tend to be suppressed under the high turbulence. Even in the high turbulence case, a locus near the endwall like Curve A in Fig. 7(a) is also found along the ridge of Sh. The peak value of Sh along the locus in Fig. 7(b) is nearly the same as that along Curve A, and the peak locations in the s_s-direction in Fig. 7(a) and (b) coincide with each other. Therefore, the high turbulence, which has a significant effect on the boundary-layer separation and re-attachment near the mid-span, have a relatively minor effect on the suction-side corner vortex. However, a close comparison shows that the locus in Fig. 7(b) is located slightly closer to the endwall and less distinct in comparison with Curve A. This is an evidence that the suction-side corner vortex tends to be weakened slightly by the high turbulence. Under the high turbulence, the ridge of Sh like Curve C in Fig. 7(a) is no longer existent in Fig. 7(b), because the secondary flow along Curve C is swept away by the high turbulence. Its disappearance makes it hard to identify the valley of Sh like Curve B.

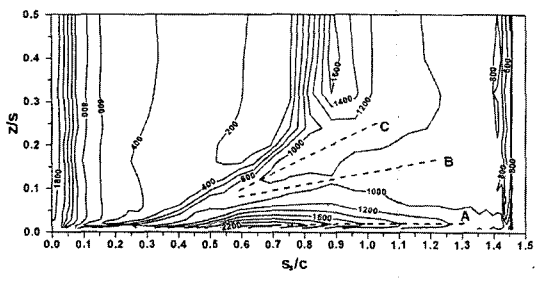

(a) Low turbulence case

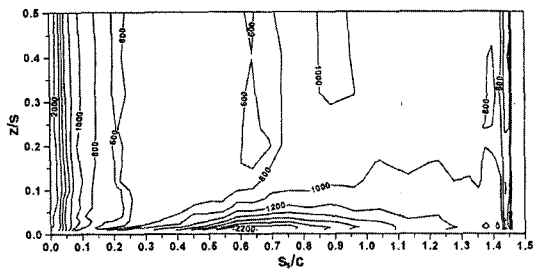

(b) High turbulence case

Fig. 7 Contours of Sh on the suction surface

Direct comparisons of Sh between the low and high turbulence cases are made in Fig. 8. The corner vortices mentioned earlier reside at $z/s=0.02$, and they are not influenced greatly by the high turbulence. Thus, mass transfers in the low and high turbulence in Fig. 8(a) are not so different from each other at this span-wise location. Regardless of z/s, Sh in the high turbulence case has a higher value than that in the low turbulence case in the leading-edge region. This is because the high turbulence always increases stagnation transport. At $z/s=0.12$, where there is no direct influence of the corner vortices, mass-transfer deviations between the low and high turbulence cases become larger. These deviations always exist in the regions where flow separation and re-attachment occur. Along the pressure surface after the inflection point, Sh decreases consistently in the low turbulence case, while Sh under the high turbulence has a nearly uniform

distribution. On the suction surface, there is a large discrepancy of Sh at between $s_s/c=0.2$ and 0.6, and Sh in this region increases significantly under the high turbulence. At higher elevation from the endwall, overall trends in Fig. 8(b) become more noticeable as in Fig. 9(c).

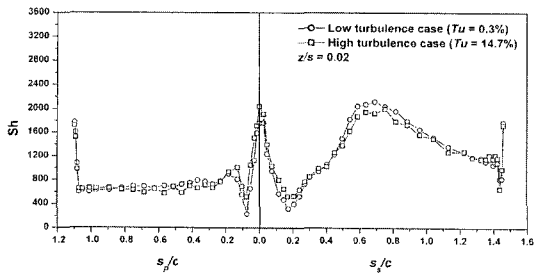

(a) $z/s=0.02$

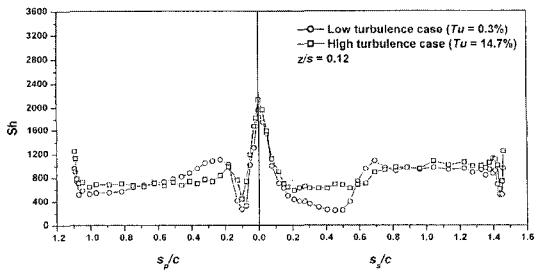

(b) $z/s=0.12$

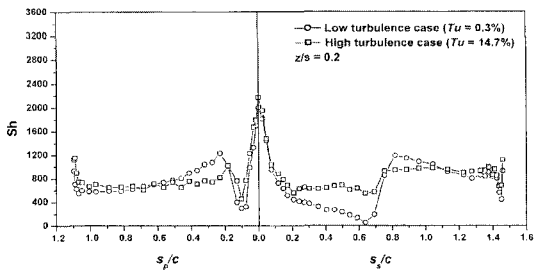

(c) $z/s=0.2$

Fig. 8 Chord-wise distributions of Sh in the three-dimensional endwall flow region

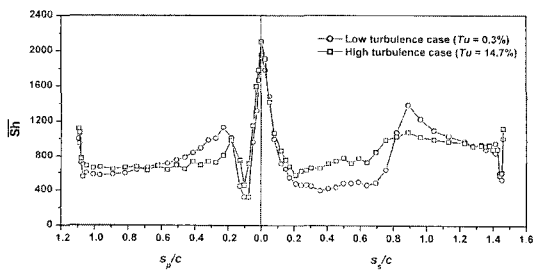

Fig. 9 Chord-wise distributions of $\overline{Sh}$

3.3 Mean Sherwood number

Sherwood number averaged in the span-wise direction, $\overline{Sh}$, is presented in Fig. 9. There is a more uniform distribution of $\overline{Sh}$ under the high turbulence. $\overline{Sh}$ in the high turbulence case has higher values in the separated zones, but has lower values in the re-attachment regions. Mean Sherwood number averaged across the entire blade surface area is given to be 787.6 and 831.8 in the low and high turbulence cases, respectively.

3.4 Comparison with previous heat-transfer data

Mehendale et al.(1994) reported Nusselt number data spanwise-averaged in the mid-span region between $z/s=0.3$ and 0.7. Their turbine rotor blade has a lower turning angle than that in this study by about 12 degree. In general, Nusselt number, Nu, can be obtained from Sh by using Eq. (2). In Fig. 10, present $(Sh/Re^{0.5})(Pr/Sc)^{1/3}$, which is equivalent to $Nu/Re^{0.5}$ in a laminar boundary-layer flow, is compared with their $Nu/Re^{0.5}$ data. This comparison shows that the two results in the stagnation region have very good agreements in both the low and high turbulence cases. Away from the leading edge, however, there exist big differences between the two results. This is because the two blades have different profiles and heat transfer experiment basically has a wall-conduction error that tends to make local gradient milder, particularly in separation and reattachment regions as well as in trailing-edge separation zones. Furthermore, we assumed that there is only a laminar boundary layer all over the blade surface in applying the

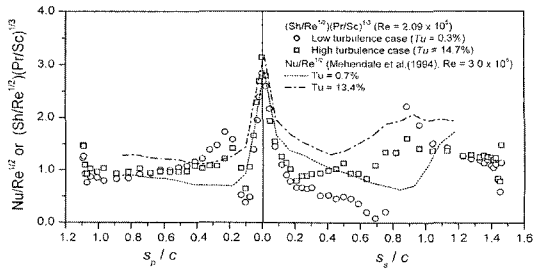

Fig. 10 Comparison of present mid-span results with those of Mehendale et al.(1994)

heat and mass transfer analogy.

4. Conclusions

The effects of a combustor-level high free-stream turbulence on the convective transport on the blade surface have been investigated for a linear high-turning turbine rotor cascade. Major new findings are summarized as follows.

(1) There is no considerable discrepancy in heat/mass transfer between the low and high turbulence cases near the endwall. As departing from the endwall, however, the deviation between the two cases becomes larger, particularly in the region where flow separation and re-attachment occur. In general, the high turbulence tends to make the blade surface heat/mass transfer more uniform.

(2) The boundary-layer flow separations and re-attachments on the suction surface as well as near the inflection point on the pressure surface seem to be suppressed under the high turbulence. There are some evidences that the endwall vortices tend to be weakened under the high turbulence.

(3) Under the high turbulence, the heat/mass transfer distribution on the entire pressure surface become nearly one-dimensional, and there exists a large area of uniform heat/mass transfer in the region between the mid-chord and trailing edge on the pressure surface.

(4) On the suction surface, a trace with steep mass-transfer gradient in the form of an alphabet "D" is hardly found in the high turbulence case. The high turbulence results in only a minor effect on the suction-side blade heat/mass transfer near the endwall.

References

Abernethy, R. B., Benedict, R. P. and Dowdell, R. B., 1985, "ASME Measurement Uncertainty," *ASME Journal of Fluids Engineering*, Vol. 107, pp. 161~164.

Bayley, F. J. and Priddy, W. J., 1981, "Effects of Free-stream Turbulence Intensity and Frequency on Heat Transfer to Turbine Blading," *ASME Journal of Turbomachinery*, Vol. 103, pp. 60~64.

Chen, P. H. and Goldstein, R. J., 1992, "Convective Transport Phenomena on the Suction Surface of a Turbine Blade Including the Influence of Secondary Flows Near the Endwall," *ASME Journal of Turbomachinery*, Vol. 114, pp. 776~787.

Goebel, S. G., Abuaf, N., Lovett, J. A. and Lee, C. P., 1993, "Measurements of Combustor Velocity and Turbulence Profile," *ASME Paper* No. 93-GT-228.

Goldstein, R. J. and Cho, H. H., 1995, "A Review of Mass Transfer Measurements Using Naphthalene Sublimation," *Experimental Thermal and Fluid Science*, Vol. 10, pp. 416~434.

Goldstein, R. J., Wang, H. P. and Jabbari, M. Y., 1995, "The Influence of Secondary Flows Near the Endwall and Boundary Layer Disturbance on Convective Transport From a Turbine Blade," *ASME Journal of Turbomachinery*, Vol. 117, pp. 657~665.

Graziani, R. A., Blair, M. F., Taylor, J. R. and Mayle, R. E., 1980. "An Experimental Study of Endwall and Airfoil Surface Heat Transfer in a Large Scale Turbine Blade Cascade," *ASME Journal of Engineering for Power*, Vol. 102, pp. 257~267.

Jun, S. B., 2000, Measurements of Endwall Heat (Mass) Transfer Coefficient in a Linear Turbine Cascade Using Naphthalene Sublimation Technique, MS thesis, Kumoh National Institute of Technology.

Koutmos, P. and McGuirk, J. J., 1989, "Isothermal Flow in a Gas Turbine Combustor — A Benchmark Experimental Study," *Experiments in Fluids*, Vol. 7, pp. 344~354.

Lee, S. W., Jun, S. B., Park, B. K. and Lee, J. S., 2004, "Effects of Combustor-Level High Inlet Turbulence on the Endwall Flow and Heat/Mass Transfer of a High-Turning Turbine Rotor Cascade," *KSME International Journal*, Vol. 18, pp. 1435~1450.

Mehendale, A. B., Ekkad, S. V. and Han, J. C., 1994, "Mainstream Turbulence Effect on Film Effectiveness and Heat Transfer Coefficient of a

Gas Turbine Blade with Air and CO_2 Film Injection," *Int. J. Heat Mass Transfer*, Vol. 37, pp. 2707~2714.

STP 470A, 1974, Manual on the Use of Thermocouples in Temperature Measurement, published by ASTM.

Wang, H. P., Goldstein, R. J. and Olson, S. J., 1999, "Effect of High Free-Stream Turbulence With Large Length Scale on Blade Heat/Mass Transfer," *ASME Journal of Turbomachinery*, Vol. 121, pp. 217~224.

Wang, H. P., Olson, S. J., Goldstein, R. J. and Eckert, E. R. J., 1997, "Flow Visualization in a Linear Turbine Cascade of High Performance Turbine Blade," *ASME Journal of Turbomachinery*, Vol. 119, pp. 1~8.